Electronic Supplementary Material (ESI) for Nanoscale.
This journal is © The Royal Society of Chemistry 2020

Electronic supplementary information (ESI) for

Seed-mediated growth of heterostructured $Cu_{1.94}S$-MS (M=Zn, Cd, Mn) and alloyed $CuNS_2$ (N=In, Ga) nanocrystals with structure- and composition-dependent photocatalytic hydrogen evolution

Dongxu Zhu,[a] Haihang Ye,[b,*] Zheming Liu,[a] Jun Liu,[b,c] Hao Fu,[a] Yanbin Huang,[b,c] Feng Teng,[a] Zhijie Wang[b,c*] and Aiwei Tang[a,*]

[a]Key Laboratory of Luminescence and Optical Information, Ministry of Education, School of Science, Beijing JiaoTong University, Beijing 100044, China.

[b]Mechanical Engineering Department, University of Texas at Dallas, Richardson, Texas 75080, USA

[c]Key Laboratory of Semiconductor Materials Science, Beijing Key Laboratory of Low Dimensional Semiconductor Materials and Devices, Institute of Semiconductors, Chinese Academy of Sciences, Beijing, 100083, China.

[d]Center of Materials Science and Optoelectronics Engineering, University of Chinese Academy of Sciences, Beijing, 100049, China.

***Corresponding authors.**

Email addresses: Aiwei Tang, E-mail: awtang@bjtu.edu.cn.

Zhijie Wang, E-mail: wangzj@semi.ac.cn.

Haihang Ye, E-mail: Haihang.Ye@utdallas.edu.

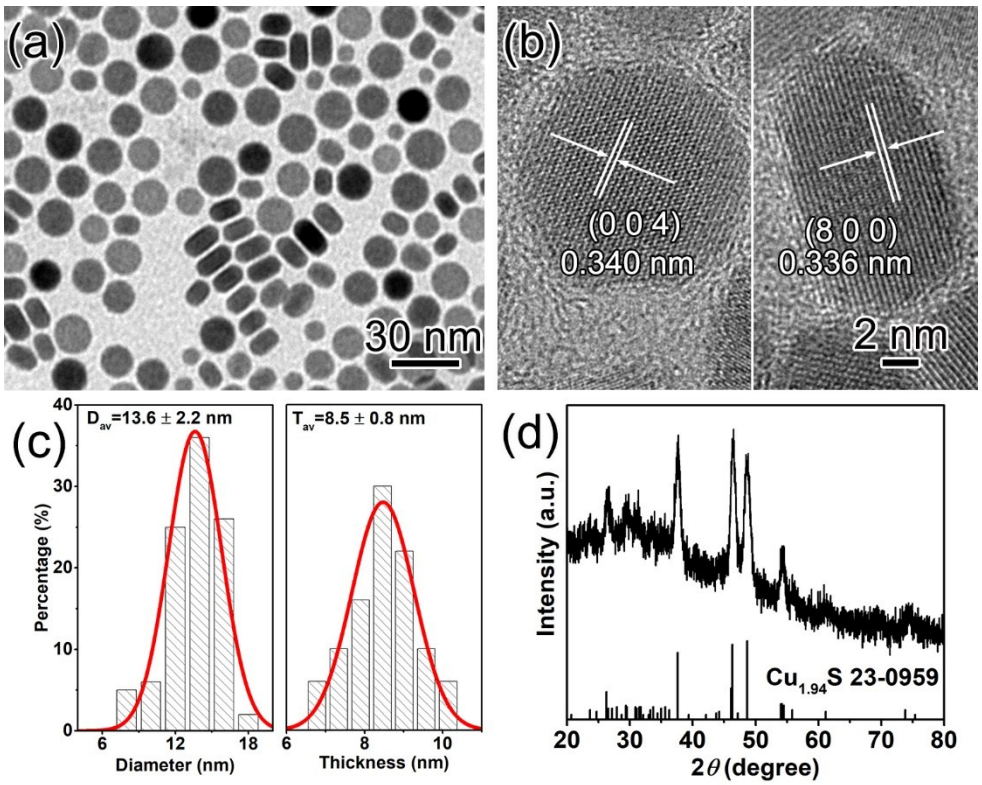

Figure S1. (a) The TEM image of $Cu_{1.94}S$ NCs; (b) the corresponding HRTEM images; (c) the size distribution of diameter and thickness; (d) the XRD pattern, the bottom lines represent the diffraction lines of standard monoclinic $Cu_{1.94}S$ (JCPDS no.23-0959).

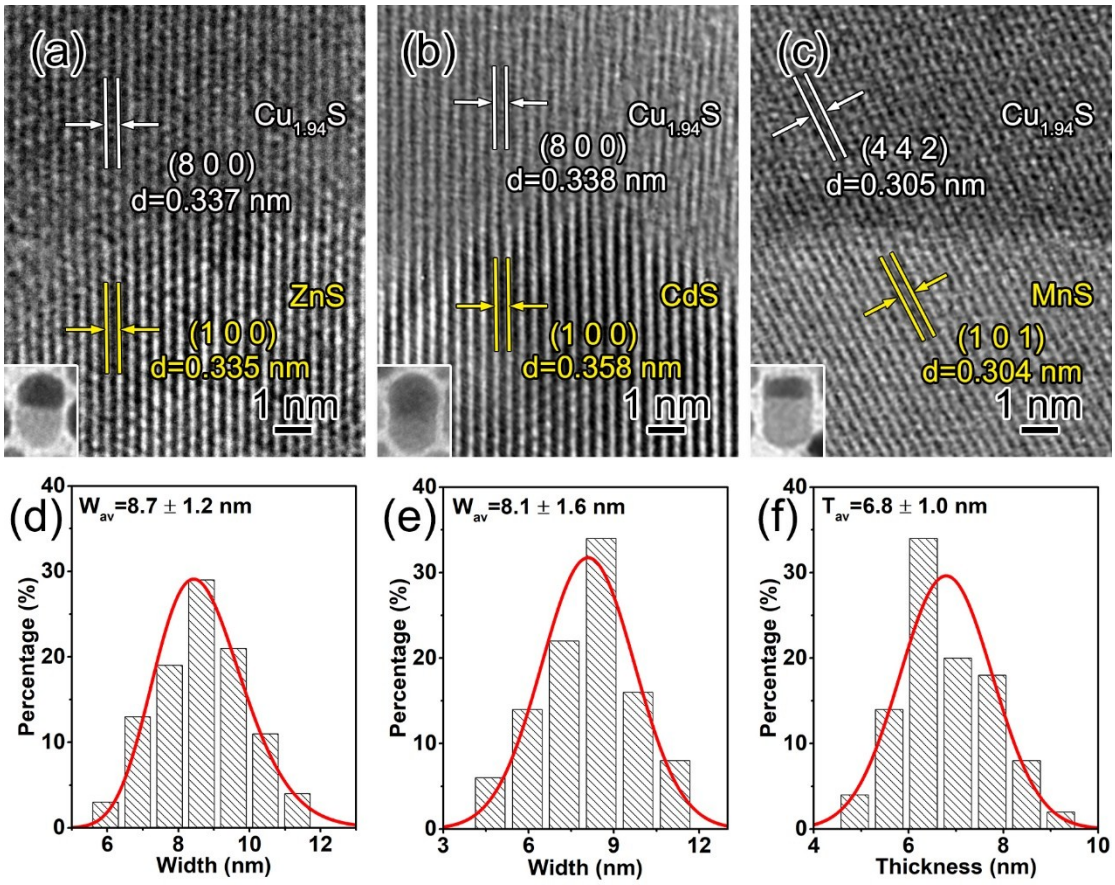

Figure S2. The HRTEM images of (a) $Cu_{1.94}S$-ZnS HNCs, (b) $Cu_{1.94}S$-CdS HNCs and (c) $Cu_{1.94}S$-MnS HNCs, and the insets are the corresponding TEM images of a single nanocrystal; the corresponding size distribution of (d) width, (e) width, (f) thickness of $Cu_{1.94}S$ seeds.

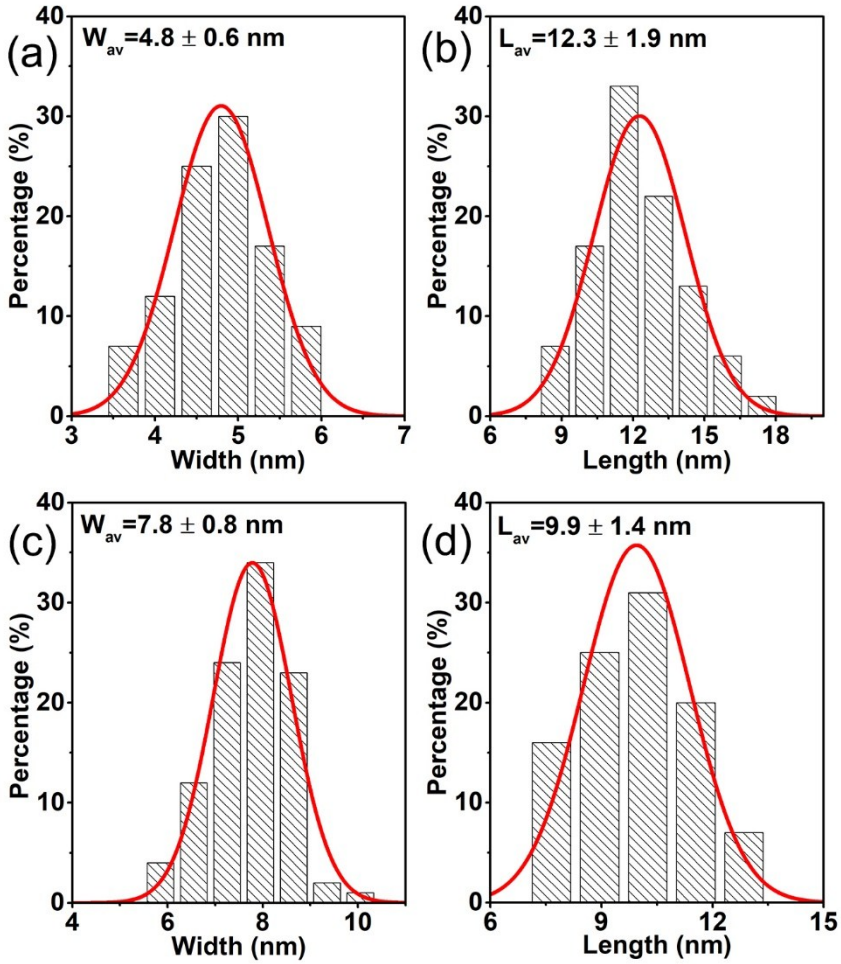

Figure S3. The size distribution of width and length of (a, b) $CuGaS_2$ ANCs and (c, d) $CuInS_2$ ANCs. W=width and L=length.

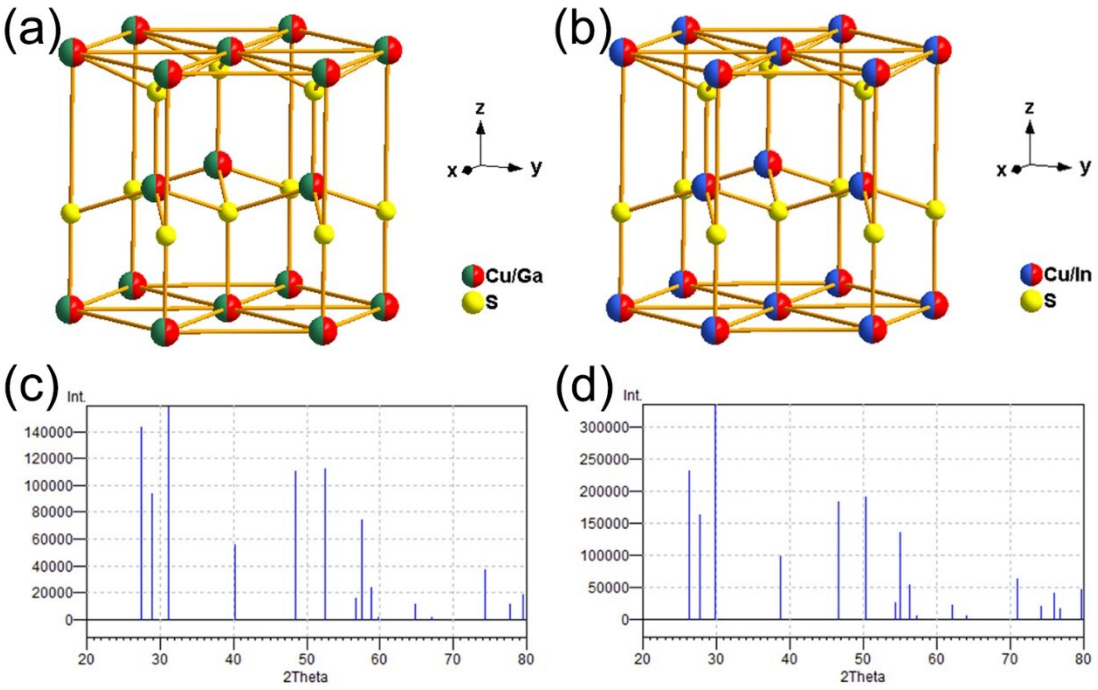

Figure S4. The schematic models of the crystal structure of (a) wurtzite $CuGaS_2$ and (b) $CuInS_2$, and the red, dark green, blue, yellow represent copper, gallium, indium and sulfur element, respectively; (c) the simulated XRD pattern of $CuGaS_2$ and (d) the simulated XRD pattern of $CuInS_2$.

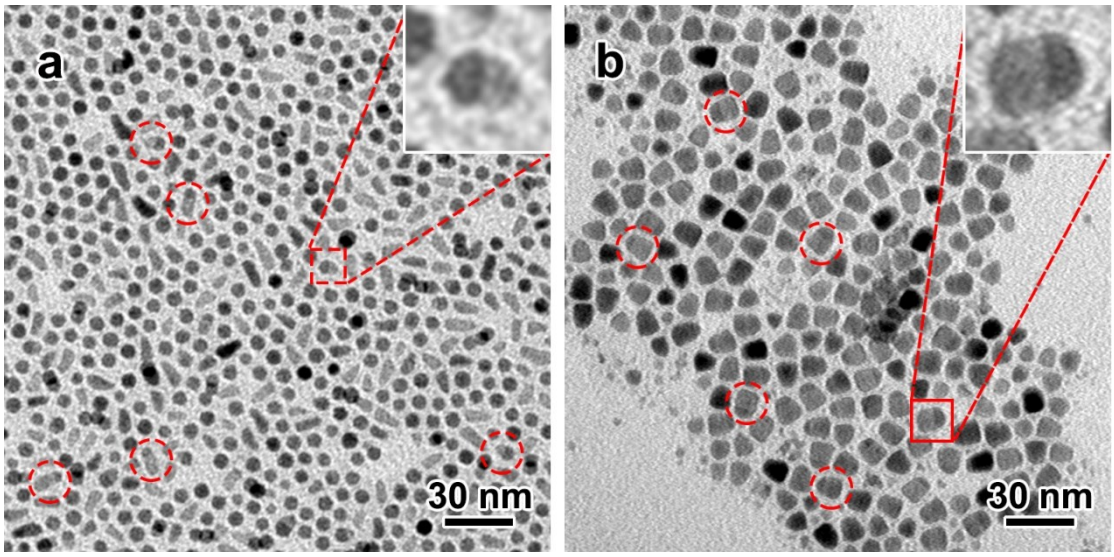

Figure S5. The TEM images in growth stage of (a) $CuGaS_2$ ANCs and (b) $CuInS_2$ ANCs, and the insets are the corresponding amplified TEM image of the heterostructure NC.

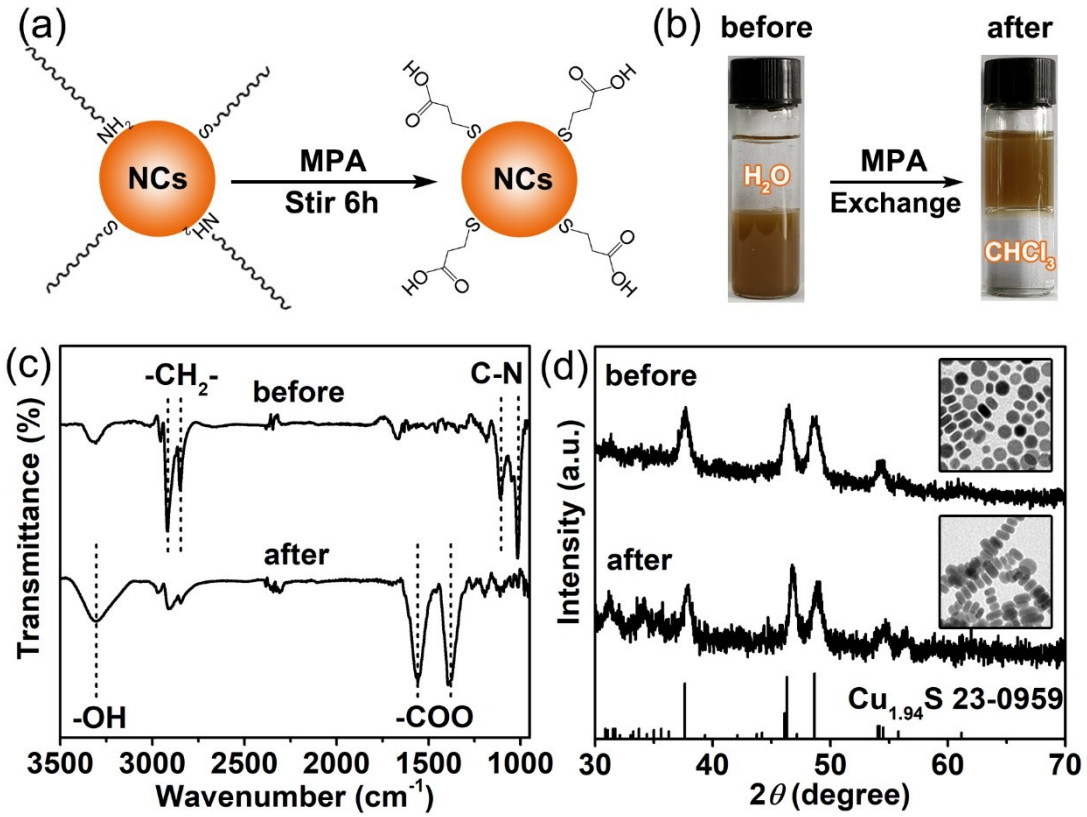

Figure S6. (a) Schematic illustration of the phase transfer of $Cu_{1.94}S$ NCs through the ligand exchange; (b) digital picture of $Cu_{1.94}S$ NCs before and after ligand exchange from chloroform (left) to water (right); (c) the FTIR spectra of $Cu_{1.94}S$ NCs before and after ligand exchange; (d) the XRD pattans inset with TEM images of $Cu_{1.94}S$ NCs before and after ligand exchange, and the bottom lines represent the diffraction lines of monoclinic $Cu_{1.94}S$ (JCPDS no.23-0959).

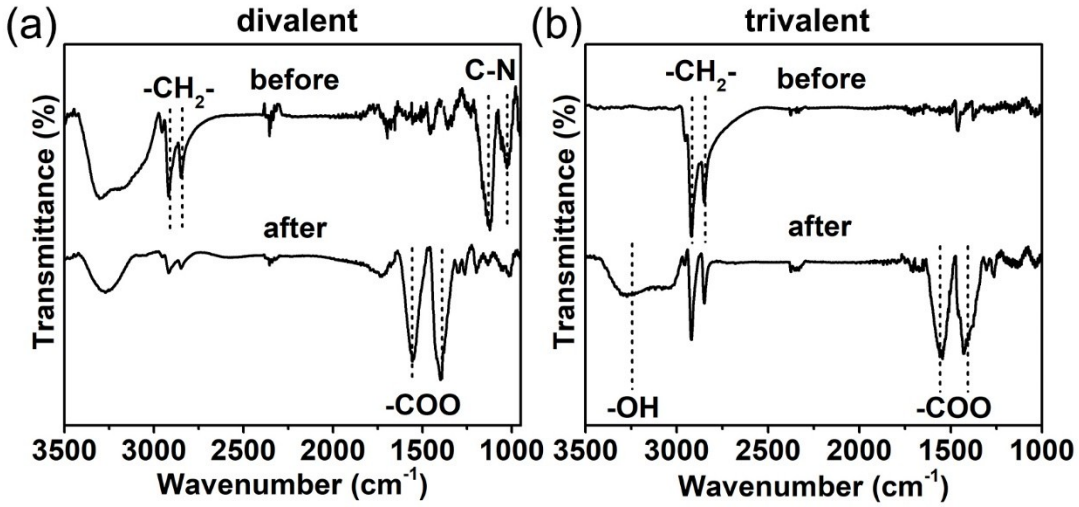

Figure S7. The FTIR spectra of (a) $Cu_{1.94}S$-CdS HNC, representing for HNCs formed by inducing divalent cation, and (b) $CuGaS_2$ ANCs, representing for ANCs formed by inducing trivalent cation.

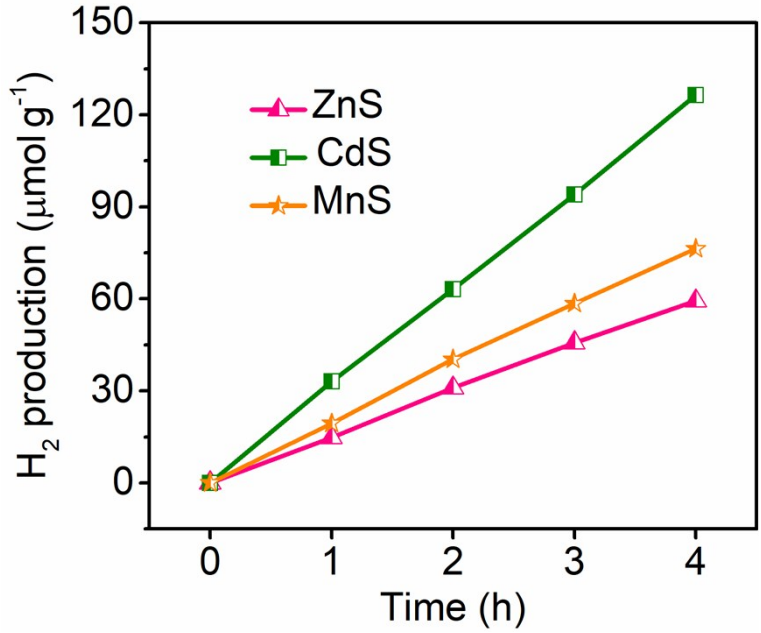

Figure S8. The hydrogen production of ZnS NCs (pink), CdS NCs(green) and MnS NCs(orange) under simulated solar light (100 mW·cm^{-2}).

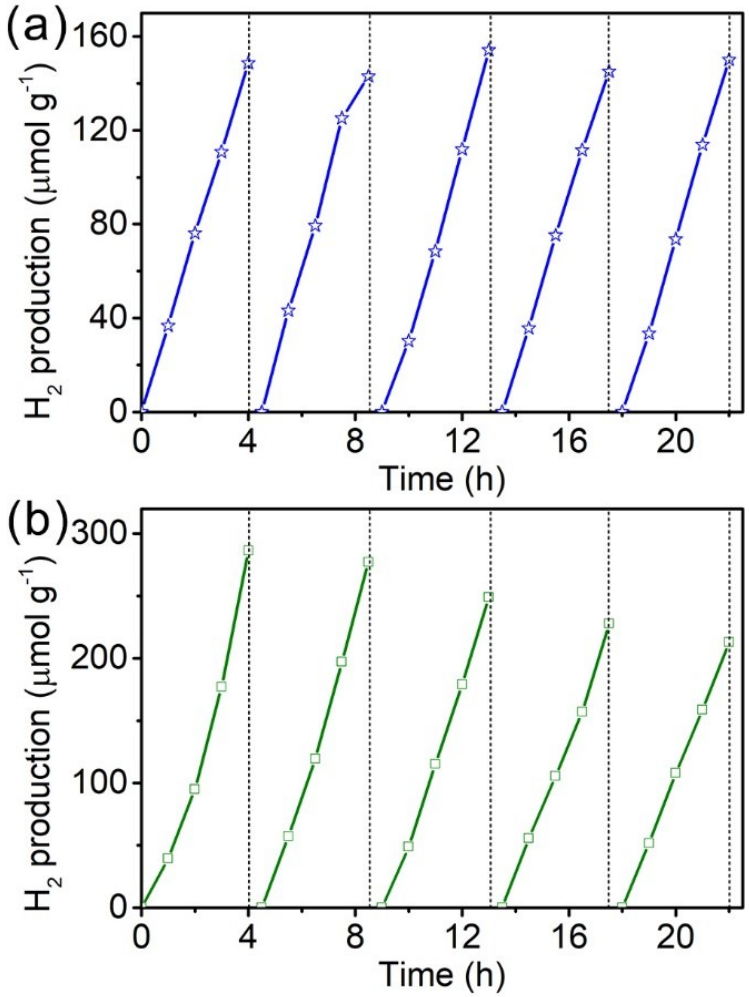

Figure S9. Cycling tests of hydrogen production of (a) $CuGaS_2$ ANCs and (b) $Cu_{1.94}S$-CdS HNCs.

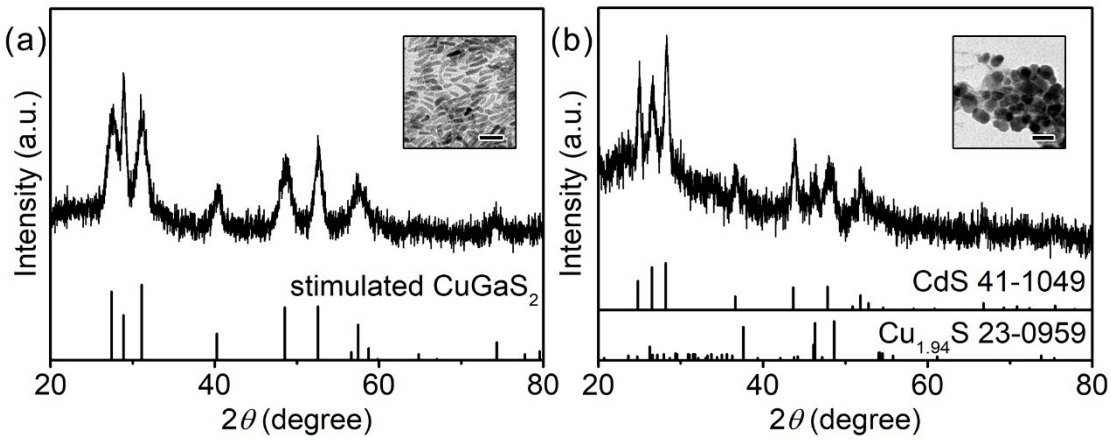

Figure S10. XRD patterns and corresponding TEM images of (a) $CuGaS_2$ ANCs and (b) $Cu_{1.94}S$-CdS HNCs after cycling tests. The TEM inset images have a 30 nm scale bar. The bottom lines represent the diffraction lines of simulated wurtzite $CuGaS_2$, the diffraction lines of standard wurtzite CdS (JCPDS no.41-1049) and monoclinic Cu1.94S (JCPDS no.23-0959).

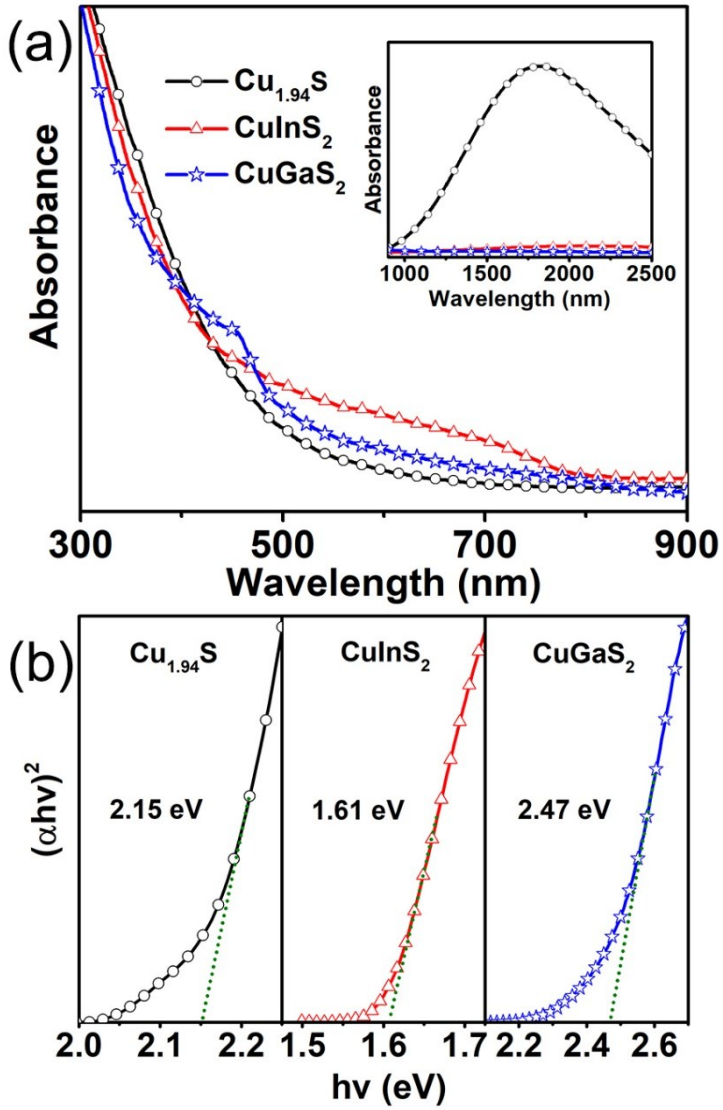

Figure S11. (a) UV-Vis absorption spectrum of $Cu_{1.94}S$ NCs, $CuInS_2$ ANCs and $CuGaS_2$ ANCs, and the inset shows the corresponding vis-NIR absorption spectrum; (b) the plot of $(\alpha hv)^2$ versus the photo energy.

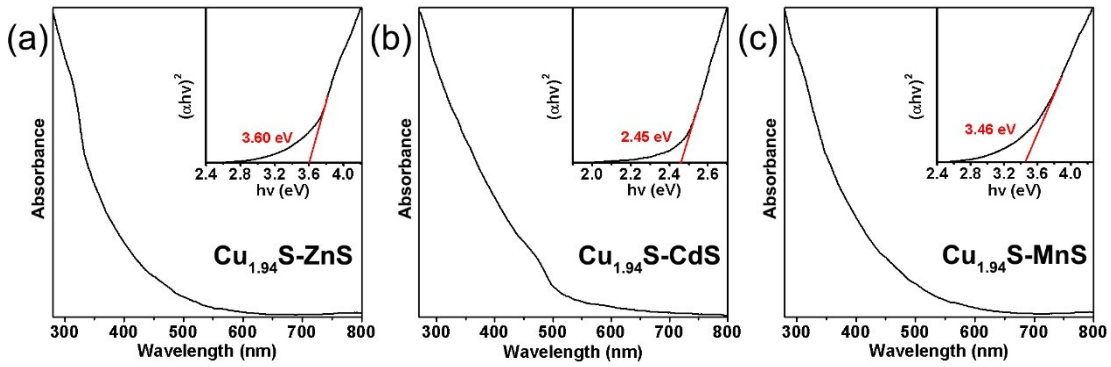

Figure S12. UV-Vis absorption spectrum of (a) $Cu_{1.94}S$-ZnS HNCs, (b) $Cu_{1.94}S$-CdS HNCs, (c) $Cu_{1.94}S$-MnS HNCs. The insets show the corresponding plot of $(\alpha h\nu)^2$ versus the photon energy.

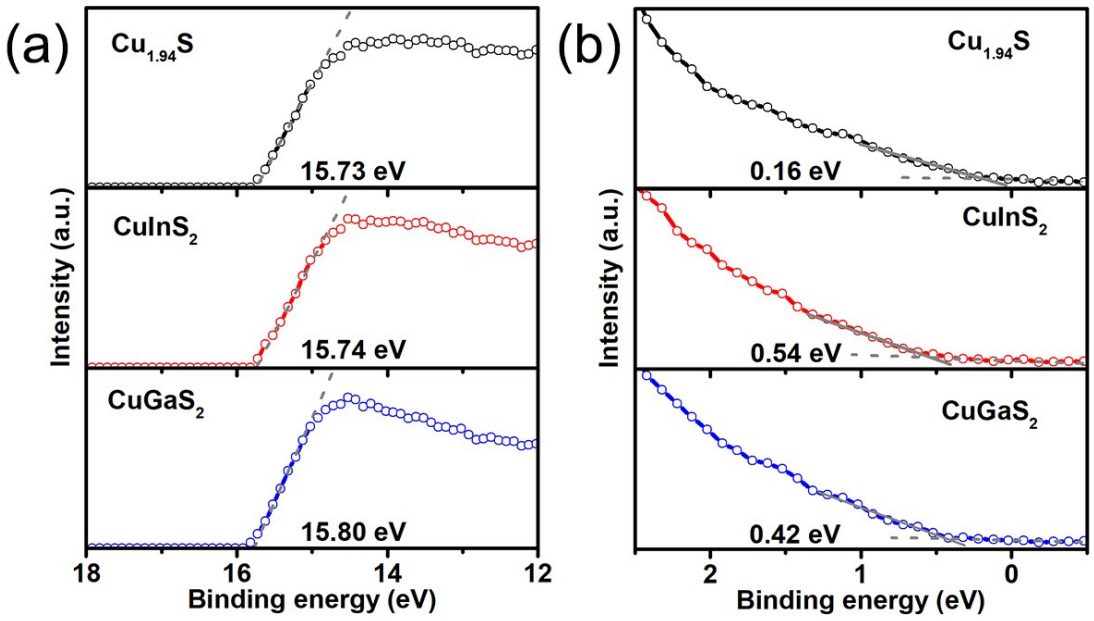

Figure S13. UPS spectra of (a) the high-binding energy secondary electron cut-off regions and (b) the valence-band edge regions of $Cu_{1.94}S$ NCs, $CuInS_2$ ANCs and $CuGaS_2$ ANCs.

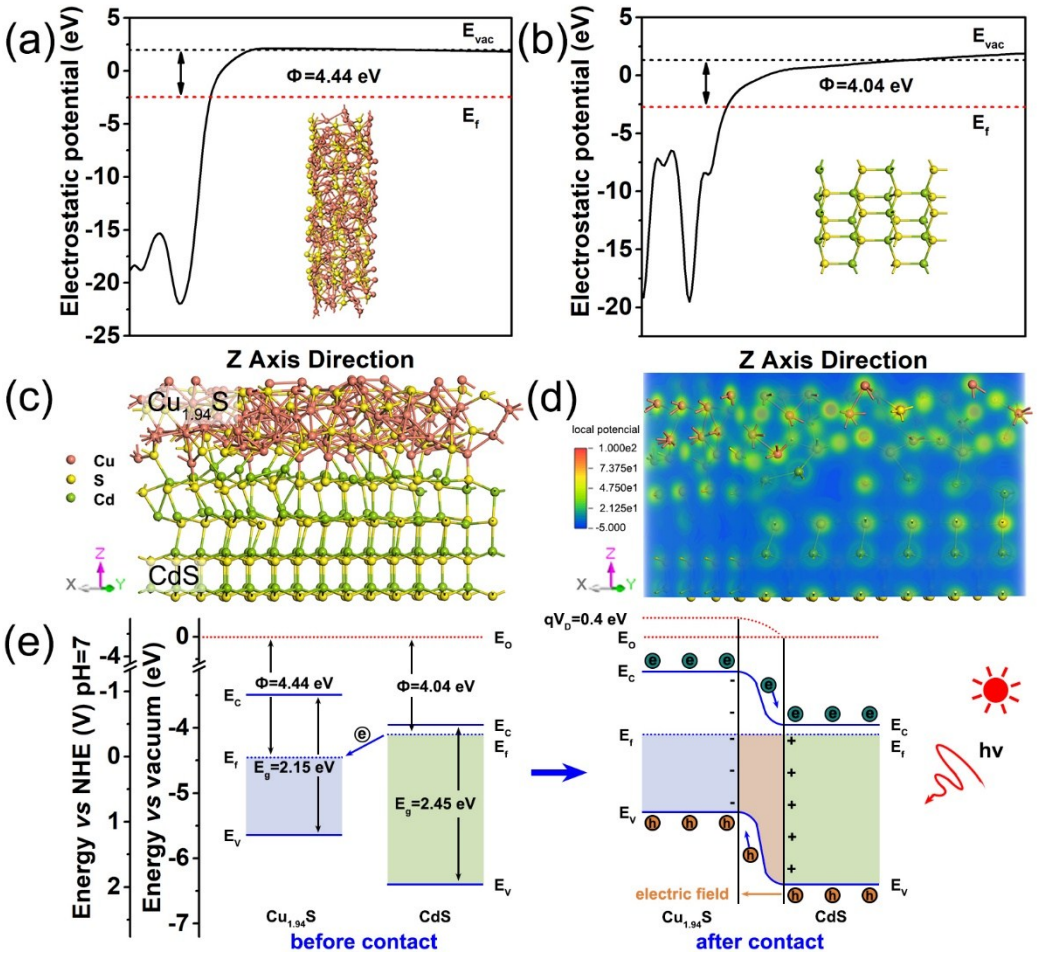

Figure S14. The electrostatic potential for (a) $Cu_{1.94}S$ (0 0 4) surface and (b) CdS (0 0 2) surface, and the black and red dash line denote the vacuum energy level and Fermi level. The insets show the corresponding schematic models, and the red, green and yellow spheres represent the copper, cadmium and sulfur atom. (c) the schematic model and (d) the calculated local potential diagram of $Cu_{1.94}S$ (0 0 4)-CdS (0 0 2) interfaces; (e) schematic illustration of band alignment and charge separation at the interface of $Cu_{1.94}S$ (0 0 4)-CdS (0 0 2). Φ, V_{ac}, E_f, E_C, E_V, E_g are the work function, vacuum level, Fermi level, conduction band minimum, valence band maximum and band gap.

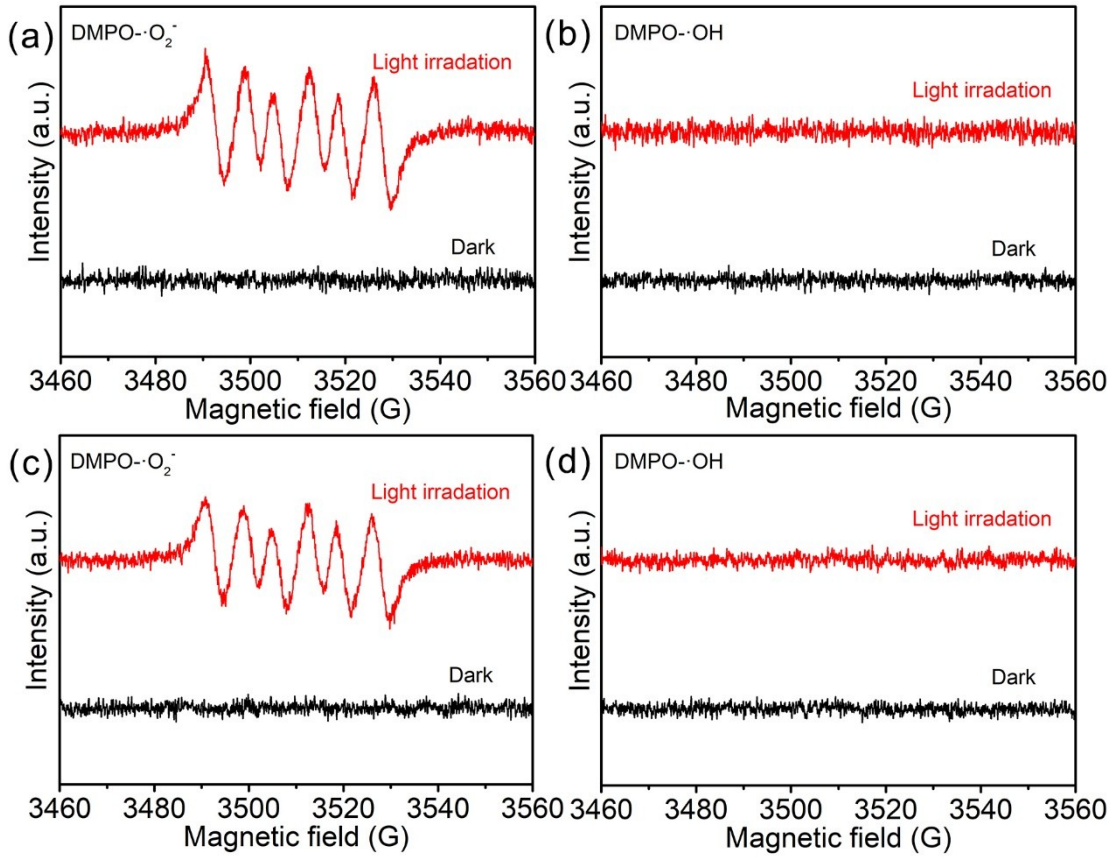

Figure S15. DMPO spin-trapping ESR spectra of $Cu_{1.94}S$-ZnS HNCs (a) DMPO-$^{\bullet}O_2^-$ and (b)DMPO-$^{\bullet}OH$, $Cu_{1.94}S$-CdS HNCs (c) DMPO-$^{\bullet}O_2^-$ and (d)DMPO-$^{\bullet}OH$.

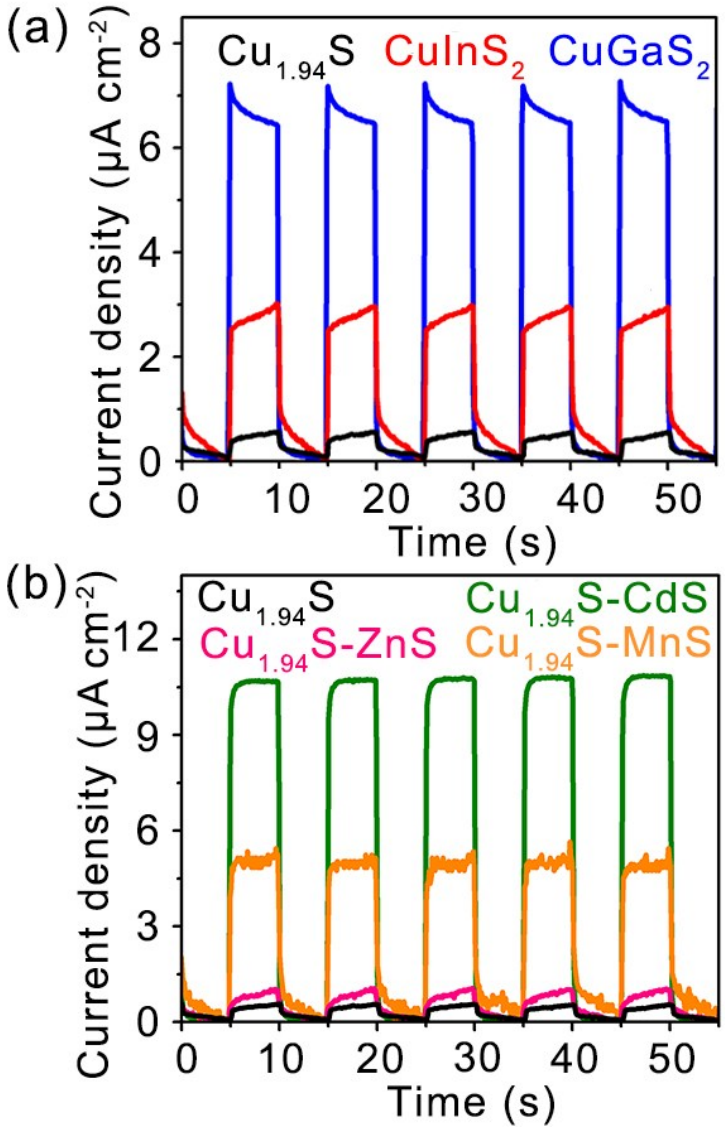

Figure S16. The transient photocurrent response at the bias of -0.4 V *vs*. Ag/AgCl $Cu_{1.94}S$ NCs (black), $CuInS_2$ ANCs (red) and $CuGaS_2$ ANCs (blue); (b) $Cu_{1.94}S$ NCs (black), $Cu_{1.94}S$-ZnS HNCs (pink), $Cu_{1.94}S$-CdS HNCs (green) and $Cu_{1.94}S$-MnS HNCs (orange).

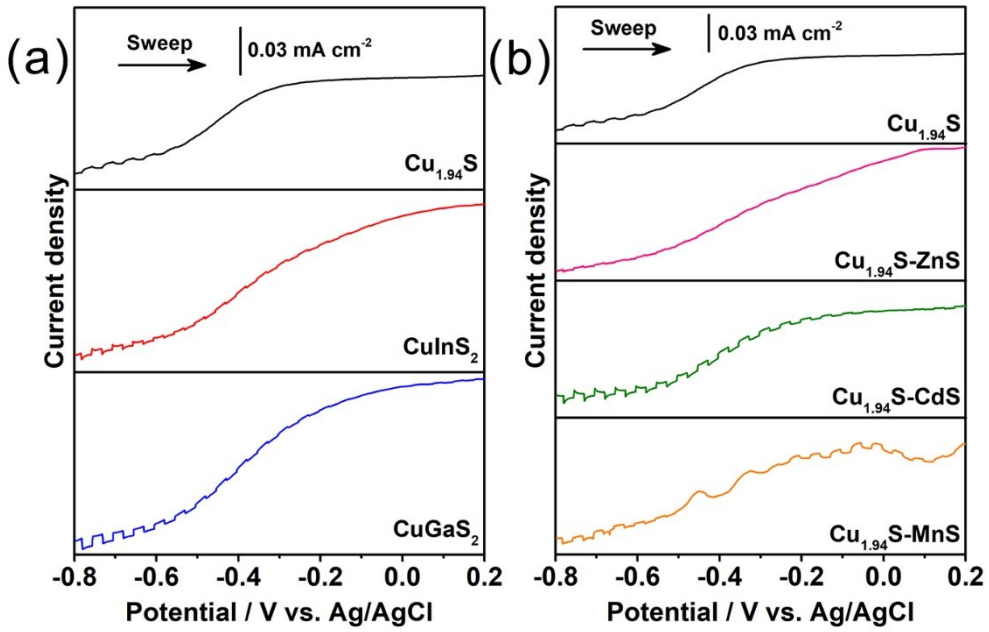

Figure S17. Linear sweep voltammograms (LSV) of (a) $Cu_{1.94}S$ NC, $CuInS_2$ ANCs and $CuGaS_2$ ANCs; (b) $Cu_{1.94}S$ NC, $Cu_{1.94}S$-ZnS HNCs, $Cu_{1.94}S$-CdS HNCs and $Cu_{1.94}S$-MnS HNCs under chopped illumination.

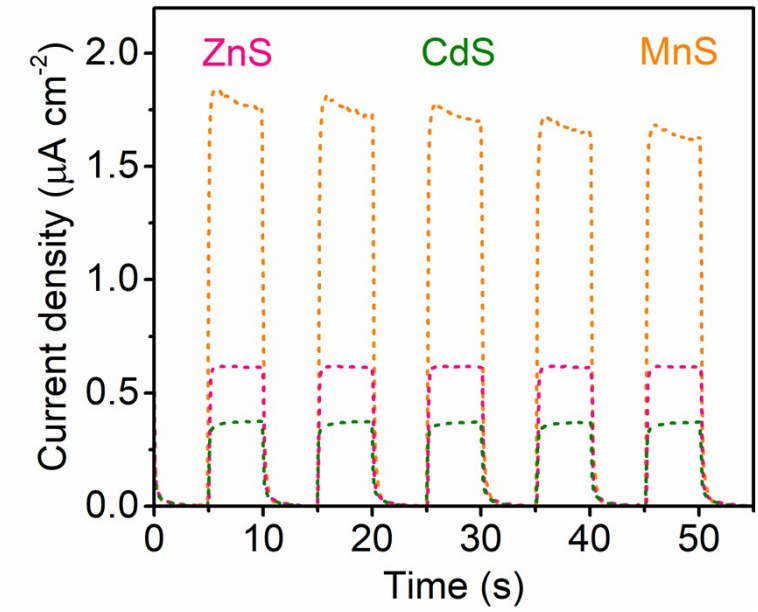

Figure S18. The transient photocurrent response of ZnS NCs (pink dash line), CdS NCs (green dash line) and MnS NCs (orange dash line) at the bias of -0.4 V *vs*. Ag/AgCl.

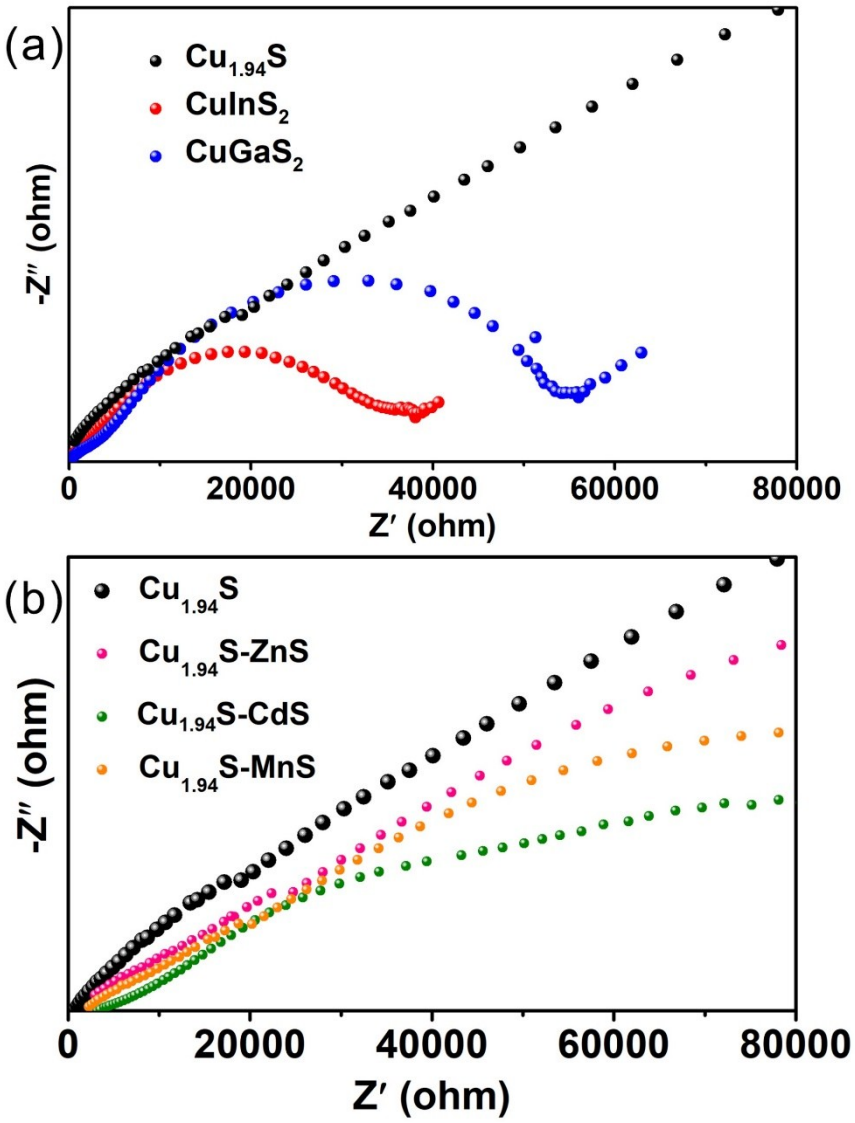

Figure S19. Nyquist plots of (a) $Cu_{1.94}S$ NC, $CuInS_2$ ANCs and $CuGaS_2$ ANCs; (b) $Cu_{1.94}S$ NC, $Cu_{1.94}S$-ZnS HNCs, $Cu_{1.94}S$-CdS HNCs and $Cu_{1.94}S$-MnS HNCs.

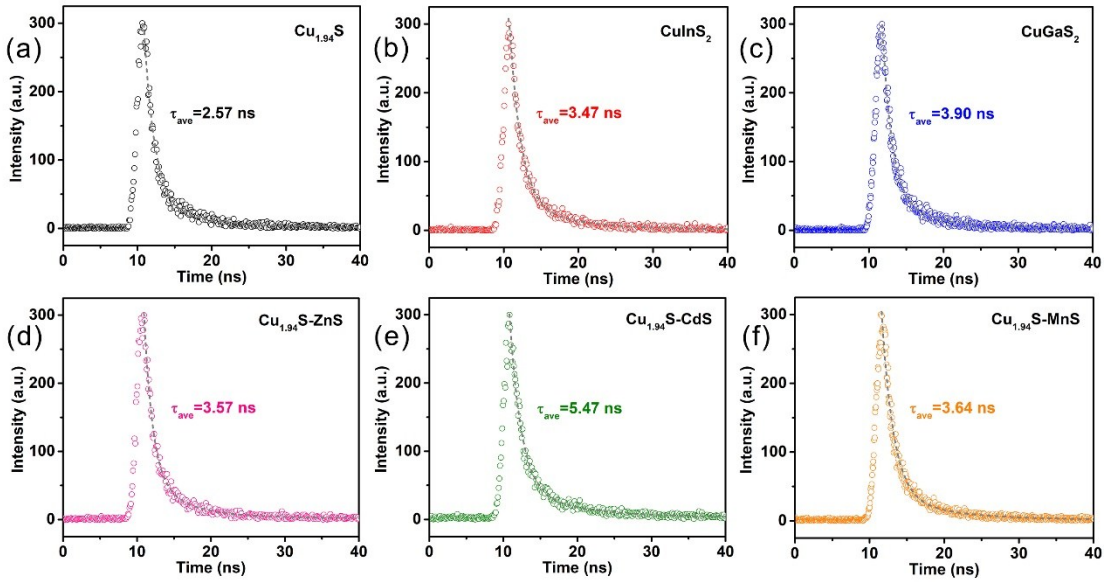

Figure S20. Experimental (dots) and fitting (line) results of time-resolved PL decay curves of (a) $Cu_{1.94}S$ NCs, (b) $CuInS_2$ ANCs, (c) $CuGaS_2$ ANCs, (d) $Cu_{1.94}S$-ZnS HNCs, (e) $Cu_{1.94}S$-CdS HNCs and (f) $Cu_{1.94}S$-MnS HNCs.

The PL lifetime was fitted by triexponential decay function, the average lifetime was calculated by the following equation[1]:

$$\tau_{ave} = \frac{A_1\tau_1^2 + A_2\tau_2^2 + A_3\tau_3^2}{A_1\tau_1 + A_2\tau_2 + A_3\tau_3}$$

Where, τ_1, τ_2 and τ_3 represent the emission lifetime of the decay components, and A_1, A_2 and A_3 are the corresponding amplitudes. All the information was summarized and listed in **Table S3**.

Table S1. Absolute electronegativity (χ), band gap (E_g), energy level of calculated conduction band minimum (E_c) and valence band maximum (E_v)

Sample	χ(eV)	E_g (eV)	CBM (eV) **	VBM (eV) **	Reference
ZnS	5.26	3.60	-0.98	2.62	experiment*
CdS	5.18	2.45	-0.45	1.97	experiment*
MnS	4.81	3.46	-1.36	2.10	experiment*
ZnS	5.26	3.60	-0.98	2.62	[2]
CdS	5.18	2.40	-0.46	1.94	[2]
MnS	4.81	3.00	-1.13	1.87	[2]

The value of VBM and CBM is versus the NHE (normal hydrogen electrode).

* The experimental results of wurtzite ZnS, wurtzite CdS and wurtzite MnS in this paper.

** VBM and CBM were calculated according to the following equations:

$VBM=\chi-E_e+0.5E_g$

$CBM=VBM-E_g$

E_e is the energy of free electron on the hydrogen scale (4.44 eV)

Table S2. Hydrogen production rate and transient photocurrent density of $Cu_{1.94}S$ NCs, ZnS NCs, CdS NCs, MnS NCs, $Cu_{1.94}S$-ZnS HNCs, $Cu_{1.94}S$-CdS HNCs and $Cu_{1.94}S$-MnS HNCs.

Sample	$Cu_{1.94}S$	ZnS	CdS	MnS	$Cu_{1.94}S$-ZnS	$Cu_{1.94}S$-CdS	$Cu_{1.94}S$-MnS
H_2 production rate ($\mu mol \cdot h^{-1} \cdot g^{-1}$)	20	15	32	19	24	71	34
Current density ($\mu A\ cm^{-2}$)	0.50	0.59	0.38	1.71	0.89	10.69	4.95

Table S3. Summary of information obtained from time-resolved PL decay curves

Sample	τ_1(ns)	α_1(%)*	τ_2(ns)	α_2(%)*	τ_3(ns)	α_3(%)*	τ_{ave}(ns)
$Cu_{1.94}S$	0.87	26.47	0.89	33.61	5.10	39.92	2.57
$CuInS_2$	0.79	43.79	3.40	43.19	12.70	13.02	3.47
$CuGaS_2$	0.92	50.56	3.69	37.00	16.60	12.45	3.90
$Cu_{1.94}S$-ZnS	0.76	47.90	3.37	39.19	14.65	12.90	3.57
$Cu_{1.94}S$-CdS	1.10	50.08	5.24	39.65	27.63	10.27	5.47
$Cu_{1.94}S$-MnS	0.86	44.95	3.47	40.46	12.69	14.59	3.64

* $\alpha_i=A_i\tau_i/(A_1\tau_1 +A_2\tau_2 +A_3\tau_3)$

Reference

[1] B. Zeng, F. Chen, Z. Liu, Z. Guan, X. Li, F. Teng and A. Tang, *J. Mater. Chem. C*, 2019, **7**, 1307-1315.

[2] Y. Xu and M. A. A. Schoonen, *American Mineralogist*, 2000, **85**, 543-556.